

## Structural hierarchy of $\text{NH}_4\text{V}_3\text{O}_7$ particles prepared under hydrothermal conditions

G. S. Zakharova<sup>1,2</sup>, Y. Liu<sup>3</sup>, I. S. Popov<sup>1</sup>, A. N. Enyashin<sup>1</sup>

<sup>1</sup>Institute of Solid State Chemistry UB RAS, Ekaterinburg, Russia

<sup>2</sup>Kirchhoff Institute for Physics, University of Heidelberg, Germany

<sup>3</sup>Institute of Materials Science and Engineering,

Wuhan University of Technology, PR China

enyashin@ihim.uran.ru

PACS 61.50.Ah, 61.72.Hh, 71.20.Ps

DOI 10.17586/2220-8054-2015-6-4-583-592

Despite having simple stoichiometry,  $\text{NH}_4\text{V}_3\text{O}_7$  still remains an odd compound with poorly resolved structure among the series of known ammonium vanadates. Here, a new hydrothermal synthesis of the product with explicit  $\text{NH}_4\text{V}_3\text{O}_7$  stoichiometry is evaluated. Intricate microstructure of the product is revealed as an aggregate of spherical microparticles consisting of microplatelets via scanning electron microscopy. To further guide the characterization of the  $\text{NH}_4\text{V}_3\text{O}_7$  phase, X-ray diffraction analysis and first-principle calculations were carried out to refine the structure at an atomistic level and to predict electronic properties. The results suggest a complex structural hierarchy with consequent nanodomain organization of prepared  $\text{NH}_4\text{V}_3\text{O}_7$  microplatelets.

**Keywords:** Ammonium vanadates, Hydrothermal synthesis, Microplatelets, Nanodomains, DFT calculations.

*Received: 22 June 2015*

### 1. Introduction

Mixed-valence Vanadium oxides and several of their derivatives form a wide class of functional materials for catalysts, Li-ion batteries, chemosensors, electronic and optical devices [1–3]. A rich variation of  $\text{V}^{4+}$  and  $\text{V}^{5+}$  content, the types of coordination polyhedra and their possible arrangements permit a very large variety of possible V–O frameworks and serve as great opportunity to design new advanced crystalline structures. The chemical nature of V–O frameworks enables hydrothermal (i.e. solvothermal) synthesis as the most outstanding and cost-effective method with widely varying experimental conditions for their fabrication [4,5].

The electroneutrality of a charged V–O framework can be compensated using appropriate amount of intercalated metal or complex cations, such as ammonium [6–9]. Particularly, to date, a few compounds in the family of ammonium polyvanadates are known –  $\text{NH}_4\text{V}_4\text{O}_{10}$  [9–12],  $\text{NH}_4\text{V}_4\text{O}_{14}$  [13],  $(\text{NH}_4)_2\text{V}_3\text{O}_8$  [14],  $\text{NH}_4\text{V}_3\text{O}_7$  [15]. Large  $\text{NH}_4^+$ -ions stabilize the internal pillar-like cavities within the vanadate frameworks, leading to enhanced diffusion rate of lithium ions. The latter is a necessary attribute of the cathode material for high capacity rechargeable Li-ion batteries.

Diammonium trivanadate  $(\text{NH}_4)_2\text{V}_3\text{O}_8$  crystallizes as a fresnoite structure and attracts much attention due to its magnetic properties [16,17]. Ammonium vanadium bronze,  $\text{NH}_4\text{V}_4\text{O}_{10}$  (or  $(\text{NH}_4)_{0.5}\text{V}_2\text{O}_5$ ) has a monoclinic structure. It was suggested as a potential electrode material for high capacity Li-ion batteries because of its good cyclic stability [11].  $\text{NH}_4\text{V}_4\text{O}_{10}$  showed a discharge capacity of 197.5 mAh/g remaining after 11 cycles and excellent cycling stability with the capacity retention of 81.9% after 100 cycles at 150 mAh/g [10]. Bicationic vanadium bronzes,  $(\text{NH}_4)_{0.83}\text{Na}_{0.43}\text{V}_4\text{O}_{10}\cdot 0.26\text{H}_2\text{O}$  [18] and  $(\text{NH}_4)_{0.25}\text{Na}_{0.14}\text{V}_2\text{O}_5$  [19], exhibit advanced

electrochemical properties, which might presumably be attributed to the modulation of the lattice parameters due to the co-intercalation of different cations.

Despite its simple stoichiometry,  $\text{NH}_4\text{V}_3\text{O}_7$  still remains an odd compound with a poorly resolved structure among the known ammonium vanadates. This compound has been synthesized hydrothermally using  $\text{NH}_4\text{VO}_3$ ,  $\text{CuCO}_3\cdot\text{Cu}(\text{OH})_2$  and  $\text{NH}_4\text{F}$  as precursors [15]. Yet, under the reaction conditions chosen,  $\text{NH}_4\text{V}_3\text{O}_7$  was prepared in a mixture with  $(\text{NH}_4)_2\text{V}_4\text{O}_9$  phase, which challenges some credibility of subsequent crystallographic and conductivity measurements.

In recent work, we evaluate a new hydrothermal synthesis of  $\text{NH}_4\text{V}_3\text{O}_7$  compound, which allowed the isolation of a product with explicit  $\text{NH}_4\text{V}_3\text{O}_7$  stoichiometry and with a morphology consisting of microplatelets which were assembled into spherical particles. Such a high texture does not enable us to refine the unit cell parameters. Yet, as a guide for further interpretation of the  $\text{NH}_4\text{V}_3\text{O}_7$  phase, first-principle calculations were carried out to confirm the structure at an atomistic level and to predict its electronic properties. Our calculations reveal that, fabricated  $\text{NH}_4\text{V}_3\text{O}_7$  microplatelets should have a nanodomain structure.

## 2. Experimental part

### 2.1. Chimie douce synthesis

All chemical reagents were purchased from Sigma Aldrich and used without further purification. Ammonium metavanadate  $\text{NH}_4\text{VO}_3$  was used as precursor and citric acid  $\text{C}_6\text{H}_8\text{O}_7$  was used as a mild reductant. The synthesis procedure was as follows:  $\text{NH}_4\text{VO}_3$  powder was dissolved with stirring in deionized water. Then, an appropriate amount of saturated aqueous citric acid was added drop-wise until  $4 \leq \text{pH} \leq 5.5$  is achieved. The homogenous solution was placed into a teflon-lined stainless steel autoclave and maintained at  $180\text{ }^\circ\text{C}$  for 48 hours. After cooling to room temperature, the obtained black sediment was filtered, washed with deionized water and air-dried at  $50\text{ }^\circ\text{C}$ .

### 2.2. Characterization techniques

The morphology of the powder and elemental analysis were studied by scanning electron microscope Nano-SEM (FEI) with integrated energy-dispersive X-ray microspectrometer for analysis (EDX). The product was characterized by powder X-ray diffraction (XRD) by means of Shimadzu diffractometer XRD-7000 S using  $\text{Cu K}_\alpha$  radiation. Thermogravimetry (DSC-TG) was carried out using analyzer DTA 409 PC/PG (Netzsch). The samples were heated at a rate of  $10\text{ K/min}$  up to  $800\text{ }^\circ\text{C}$  under  $\text{N}_2$ .

### 2.3. Computational details

The spin-polarized calculations of  $\text{NH}_4\text{V}_3\text{O}_7$  compound were performed within the framework of the density-functional theory (DFT) [20] using the SIESTA 2.0 implementation [21,22]. The exchange-correlation potential within the Generalized Gradient Approximation (GGA) with the Perdew-Burke-Ernzerhof parametrization was used [23]. The core electrons were treated within the frozen core approximation, applying norm-conserving Troullier–Martins pseudopotentials [24]. The valence electrons were taken as  $3d^34s^24p^0$  for V,  $2s^22p^4$  for O,  $2s^22p^3$  for N and  $1s^1$  for H. The pseudopotential core radii were chosen as  $2.34\text{ a}_B$  for  $\text{V}3d$  and  $\text{V}4s$ ,  $2.50\text{ a}_B$  for  $\text{V}4p$  states,  $1.45\text{ a}_B$  for all O states,  $1.04\text{ a}_B$  for all N states, and  $0.15\text{ a}_B$  for  $\text{H}1s$  states. In all calculations, a double- $\zeta$  polarized basis set was used. The  $k$ -point mesh was generated by the method of Monkhorst and Pack [25]. The real-space grid used for the numeric integrations was set to correspond to the energy cutoff of 300 Ry. For  $k$ -point sampling, a cutoff of  $10\text{ \AA}$  was used [26]. All calculations were performed using variable-cell and atomic

position relaxations, with convergence criteria corresponding to the maximum residual stress of 0.1 GPa for each component of the stress tensor, and the maximum residual force component of  $0.05 \text{ eV/\AA}$ .

The optimized geometry was used to calculate the XRD spectra for the radiation wavelength  $\lambda = 1.5406 \text{ \AA}$  (nickel-filtered  $\text{CuK}\alpha$  radiation). XRD spectra of nanosized  $\text{NH}_4\text{V}_3\text{O}_7$  were calculated in Debye approximation as for ensemble of monodisperse nanoparticles. The smearing of reflection profiles was approximated with correction for the isotropic atomic temperature factor and with regard to the instrumental line broadening [27].

### 3. Results and Discussion

#### 3.1. Scanning microscopy

The microstructure of synthesized ammonium trivanadate ( $\text{NH}_4\text{V}_3\text{O}_7$ ) was characterized using SEM method. The SEM data reveal an insignificant dependence of the compound's morphology on the variation of pH value in the primary reaction mixture. The samples fabricated at pH 4 consist mainly of the spherical-like particles with  $3 - 8 \mu\text{m}$  diameters (Fig. 1a). In turn, these microparticles are assembled of stochastically oriented microplatelets with thickness of  $50 - 200 \text{ nm}$  and with the characteristic edge lengths up to  $3 \mu\text{m}$  (Fig. 1b).

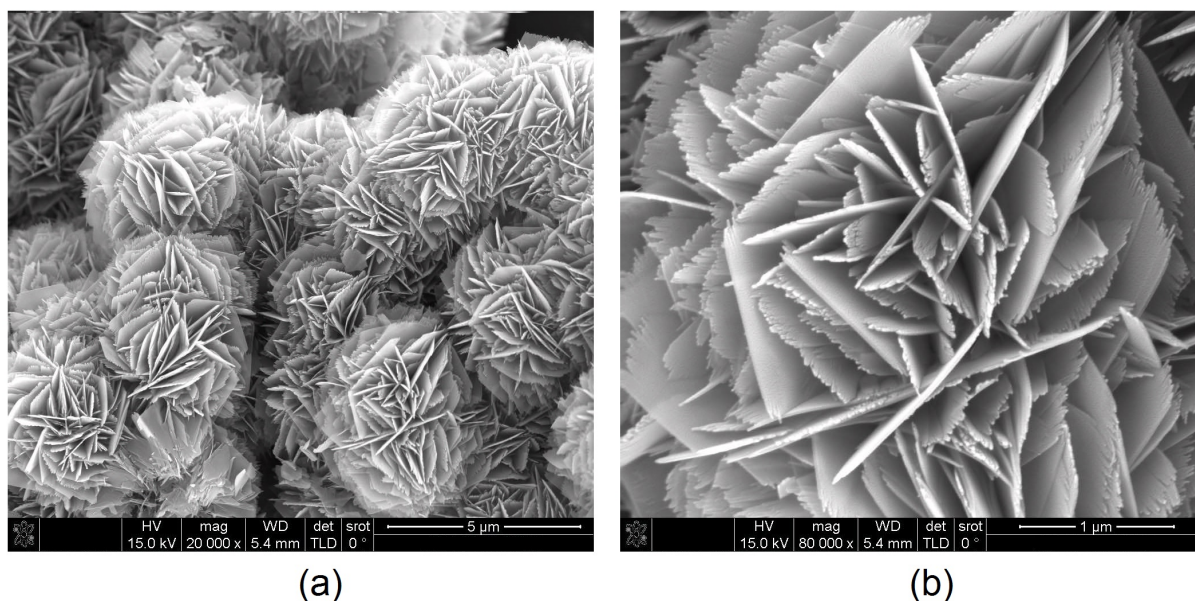


FIG. 1. SEM images of  $\text{NH}_4\text{V}_3\text{O}_7$  powder fabricated from the precursor solution with pH = 4

The morphology of  $\text{NH}_4\text{V}_3\text{O}_7$  samples isolated from the less acidic precursor solutions (pH < 4) is enriched by the separate single microplatelets. A pH value of 5.5 leads to the formation of square-like microplatelets stochastically aggregated into the particles with the diameters of  $20 - 30 \mu\text{m}$ . These platelets have the larger thickness and lengths up to  $250 - 950 \text{ nm}$  and  $5 - 15 \mu\text{m}$ , respectively.

#### 3.2. Thermogravimetric analysis

In order to determine the stoichiometry and the thermal stability of  $\text{NH}_4\text{V}_3\text{O}_7$  samples, DSC study was performed. The data of the mass loss measurements under an inert atmosphere allowed us to adjust the explicit  $\text{NH}_4\text{V}_3\text{O}_7$  stoichiometry for the prepared samples. Upon the

heating of  $\text{NH}_4\text{V}_3\text{O}_7$  powder in a stream of nitrogen, the mass loss is observed as a single stage process, which is finalized at 422 °C (Fig. 2). The decomposition of the samples is an endothermic process with the minimum corresponding to the temperature at 369 °C. In general, the decomposition of  $\text{NH}_4\text{V}_3\text{O}_7$  can be described according to the reaction

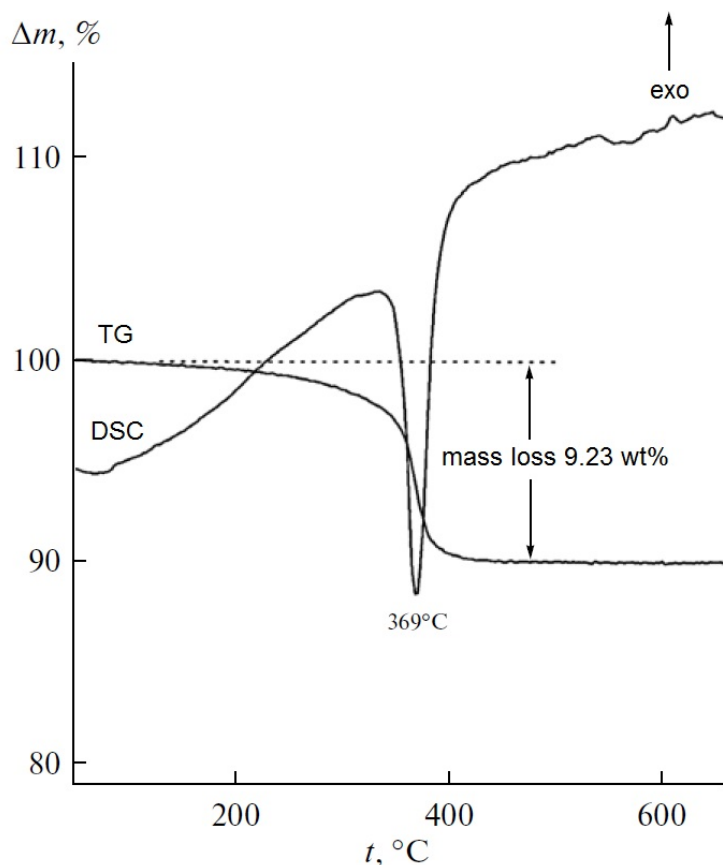
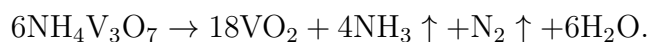


FIG. 2. TG and DSC thermogravimetric curves of  $\text{NH}_4\text{V}_3\text{O}_7$  powder decomposition under a stream of nitrogen

### 3.3. X-ray diffraction

The structure and the lattice type of experimentally observed  $\text{NH}_4\text{V}_3\text{O}_7$  phase have not been validated, yet. The former study after Trombe et al did not describe the texture of the samples in detail and no X-ray diffractogram was quoted [15]. Despite the presence of an admixture of an  $(\text{NH}_4)_2\text{V}_4\text{O}_9$  phase, the lattice parameters of  $\text{NH}_4\text{V}_3\text{O}_7$  were ascribed there to the crystal structure with its own monoclinic type and with lattice parameters of  $a = 12.198 \text{ \AA}$ ,  $b = 3.7530 \text{ \AA}$ ,  $c = 13.178 \text{ \AA}$ ,  $\beta = 100.532^\circ$ ,  $Z = 4$  (ICSD 417589). This lattice was represented as a stack of  $\text{V}_3\text{O}_7$  layers, consisting of sextuple ribbons of distorted  $\text{VO}_6$  octahedra and intercalated by ammonium cations (Fig. 3a).

XRD measurements of our samples prepared at a pH level of 4.0 – 5.5 give evidence that the crystal structure may also be described as a monoclinic phase. Yet, noticeably different lattice parameters are found:  $a = 12.247(5) \text{ \AA}$ ,  $b = 3.4233(1) \text{ \AA}$ ,  $c = 13.899(4) \text{ \AA}$ ,  $\beta = 89.72(3)^\circ$ ,

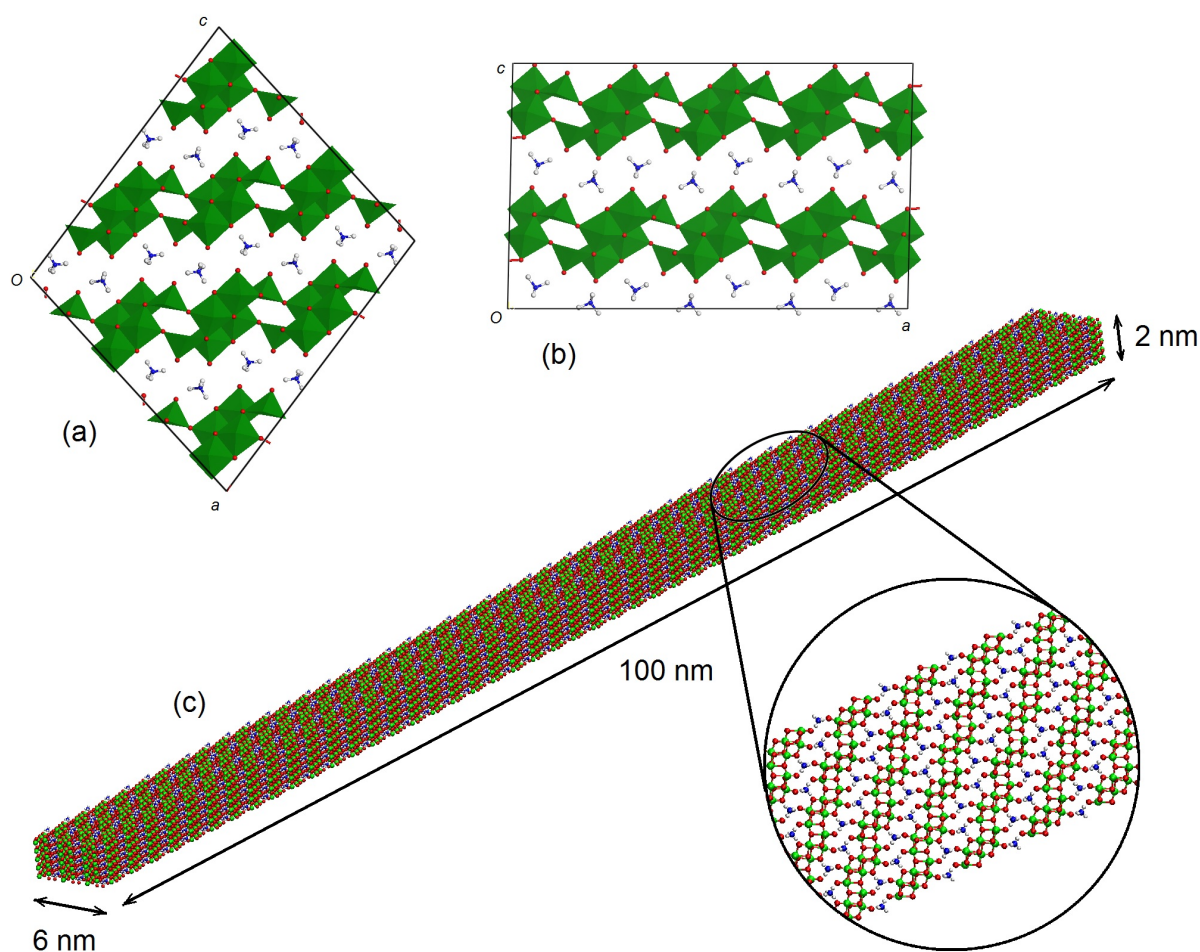


FIG. 3. Polyhedral models for DFT optimized supercells ( $Z = 16$ ) of two polytypic  $\text{NH}_4\text{V}_3\text{O}_7$  forms: (a) the most stable polytype I; (b) hypothetical and less stable polytype II (the views along  $b$ -axes are shown). Ball-and-stick model (c) demonstrates a single needle-like nanoparticle of polytype I with characteristic size  $6 \text{ nm} \times 2 \text{ nm} \times 100 \text{ nm}$  in  $a$ ,  $b$ ,  $c$  directions, respectively.

TABLE 1. Lattice parameters of  $\text{NH}_4\text{V}_3\text{O}_7$  compound concerning to experimental X-ray diffraction data in the recent work and in the work [15] versus the data for two polytypes from DFT calculations.

$\text{NH}_4\text{V}_3\text{O}_7$	$Z$	$a, \text{Å}$	$b, \text{Å}$	$c, \text{Å}$	$\beta, ^\circ$	$V, \text{Å}^3$
exp. [15]	4	12.198	3.753	13.178	100.5	593.1
exp. here	4	12.247	3.423	13.899	89.72	582.3
calc. here polytype I	4	12.211	3.832	12.886	97.8	597.5
calc. here polytype II	4	16.652	3.841	10.204	88.8	652.5

$V = 582.3(4) \text{ Å}^3$  (Table 1). At pH values  $> 5.5$ , the product possesses an admixture of  $\text{NH}_4\text{V}_4\text{O}_{10}$  compound (JCPDS 031-0075) and was not considered henceforth.

Our data suggest that the  $\text{NH}_4\text{V}_3\text{O}_7$  compound, as prepared in a recent work, should have a layered structure composed of  $(\text{V}_3\text{O}_7)$ -layers with an orientation within  $(10\bar{1})$  planes.

Regretably, further XRD structure refinement of our highly textured  $\text{NH}_4\text{V}_3\text{O}_7$  microparticles did allow a detailed view of the internal structure of the lattice. The discrepancy between our data and the previously-obtained data [15] may be attributed either to the poor characterization of highly textured samples or to the formation of a new polymorph. Hence, the first-principle calculations were employed to explore both options and to judge the crystal motif of  $\text{NH}_4\text{V}_3\text{O}_7$ .

### 3.4. Possible polytypism of $\text{NH}_4\text{V}_3\text{O}_7$

Many layered compounds are inclined to a rich polytypism due to unrestrained combination of layers' stacking. To explain the discrepancy between the recent data and earlier data [15], we surmised that another possible crystalline structure, based on the same type of  $\text{V}_3\text{O}_7$  layers may exist. Like the crystal motif suggested by Trombe et al. [15] (hereafter polytype I, Fig. 3a), the hypothetical  $\text{NH}_4\text{V}_3\text{O}_7$  polymorphic modification can be based on the same type of  $\text{V}_3\text{O}_7$  layers, yet, with every second layer shifted on  $b/2$  along [010] direction (polytype II, Fig. 3b). To validate the structure of both polytypes, optimization of their geometry has been carried out and their relative stability has been analyzed using DFT calculations.

Our DFT results are encouraging, showing that the crystal structure of polytype I has the lowest total energy and is the most stable. However, the energy of polytype II is only on 0.14 eV/ $\text{NH}_4\text{V}_3\text{O}_7$  higher than that of polytype I. Such a minor energy difference suggests the existence of at least these two polytypes or even a number of intermediate  $\text{NH}_4\text{V}_3\text{O}_7$  polytypes. The presence of numerous random dislocations along [010] direction may be not excluded, too.

The accurate first-principle calculations permit crystallographic parameter determination for both  $\text{NH}_4\text{V}_3\text{O}_7$  polytypes and comparison of them with experimental data (Table 1). Both experimental datasets do not reproduce the crystallographic properties found for hypothetical polytype II. Yet, the lattice parameters of the most stable  $\text{NH}_4\text{V}_3\text{O}_7$  polytype I may be reliably attributed to and can be found in fair agreement with former experimental values of Trombe et al. [15]. The largest deviation between calculated and these experimental lattice parameters does not exceed 2%. Thus, our experimental data cannot be seemingly assigned to the most stable crystalline phase of  $\text{NH}_4\text{V}_3\text{O}_7$ .

A more detailed insight into the structure of our highly textured samples can be performed by the comparison of experimental X-ray diffractograms with those simulated using the geometries resulted from DFT calculations. Again, theoretical diffractogram of polytype II does not reveal any similarity with the experimental data (Fig. 4). Nonetheless, theoretical diffractogram of polytype I also showed a remarkable difference. Particularly, it contains very strong reflexes missing on our experimental diffractogram at angles  $2\theta = 24^\circ$ ,  $46^\circ$  and, in general, it has a more fine profile. Such a mismatch is a clear indication of poor crystallinity for our  $\text{NH}_4\text{V}_3\text{O}_7$  product. We may surmise that the microplatelets, assembling the spherical particles of our product, should have their own internal organization at the nanoscale; e.g., every microplatelet could be an aggregate of nanoparticles or could have a nanodomain structure.

In addition, X-ray diffraction spectra of  $\text{NH}_4\text{V}_3\text{O}_7$  samples have been simulated as for the sets of monodisperse free-standing nanoparticles or nanodomains of polytype I. Routine fitting has been performed for a wide range of sizes and for several possible morphologies (compact 0D particles, 2D films, 1D needles). Despite the simplicity of all of these models, neglecting the lattice strain and possible surface reconstructions, an evident coincidence with our experimental data has been found for the case of needle-like nanoparticles with characteristic size  $6 \text{ nm} \times 2 \text{ nm} \times \sim 100\text{--}500 \text{ nm}$  along  $a$ ,  $b$ ,  $c$  directions, respectively (Fig. 3c). Some of the peaks on the profile of simulated XRD spectrum may be found as slightly shifted to the lower angles  $2\theta$ , since our DFT calculations may overestimate interlayer distances.

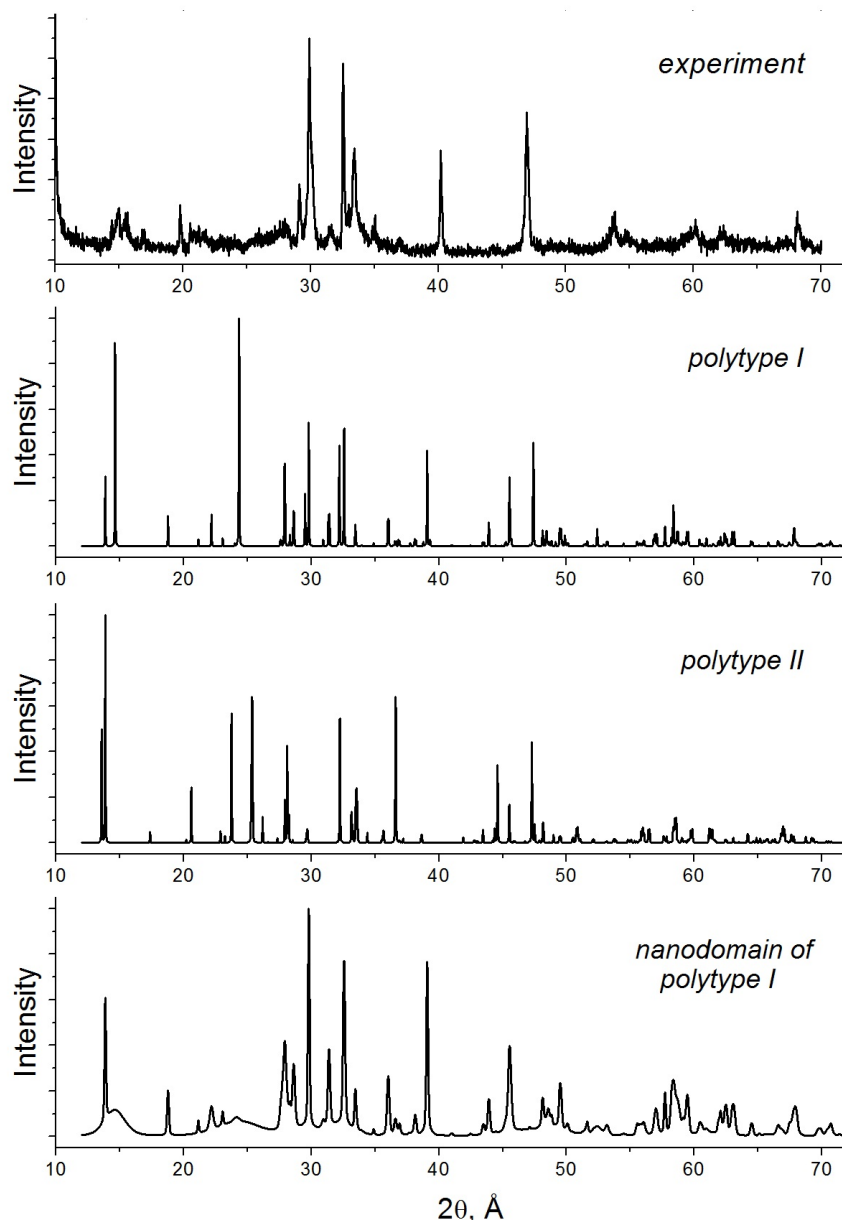


FIG. 4. Comparison between X-ray diffractograms for  $\text{NH}_4\text{V}_3\text{O}_7$  compound as observed for the samples fabricated in this work and as theoretically predicted for the monocrystals of two  $\text{NH}_4\text{V}_3\text{O}_7$  polytypic forms (I and II) and for a single needle-like nanodomain of polytype I with characteristic size of  $6 \text{ nm} \times 2 \text{ nm} \times \sim 100 \text{ nm}$  along  $a$ ,  $b$ ,  $c$  directions, respectively.

Thus, DFT calculations suggest that experimental XRD data, as obtained from our highly textured samples, should be not treated as for the monocrystal. The structural hierarchy of  $\text{NH}_4\text{V}_3\text{O}_7$  compound can be drastically enriched at the nanolevel. The  $\text{NH}_4\text{V}_3\text{O}_7$  microplatelets may have interim nanodomain structure, as the grains of polytype I and numerous low-energy dislocations, as the grain boundaries. As well, they might be assembled of free-standing  $\text{NH}_4\text{V}_3\text{O}_7$  nanoneedles. Further investigation by means of high-resolution electron microscopy could resolve the structural hierarchy of our samples in greater detail.

### 3.5. Electronic properties of $\text{NH}_4\text{V}_3\text{O}_7$

DFT calculations enable us to give prior information about the electronic properties of  $\text{NH}_4\text{V}_3\text{O}_7$  compound. The electronic density of states calculated for the most stable polytype I is visualized in Fig. 5. The studied compound,  $\text{NH}_4\text{V}_3\text{O}_7$ , should be a magnetic semiconductor with a band gap of  $\sim 0.83$  eV. The bottom of splitted conduction band has a dominant  $V3d$ -character. The top of valence band is also formed by  $V3d$ -states with an admixture of  $O2p$ -states, while the remaining wide part of the band at  $-2 \dots -6$  eV is composed predominantly of  $O2p$ -states. The deep and separated valence band at  $-7 \dots -9$  eV is formed by the mixture of  $N2p$  and  $H1s$  states.

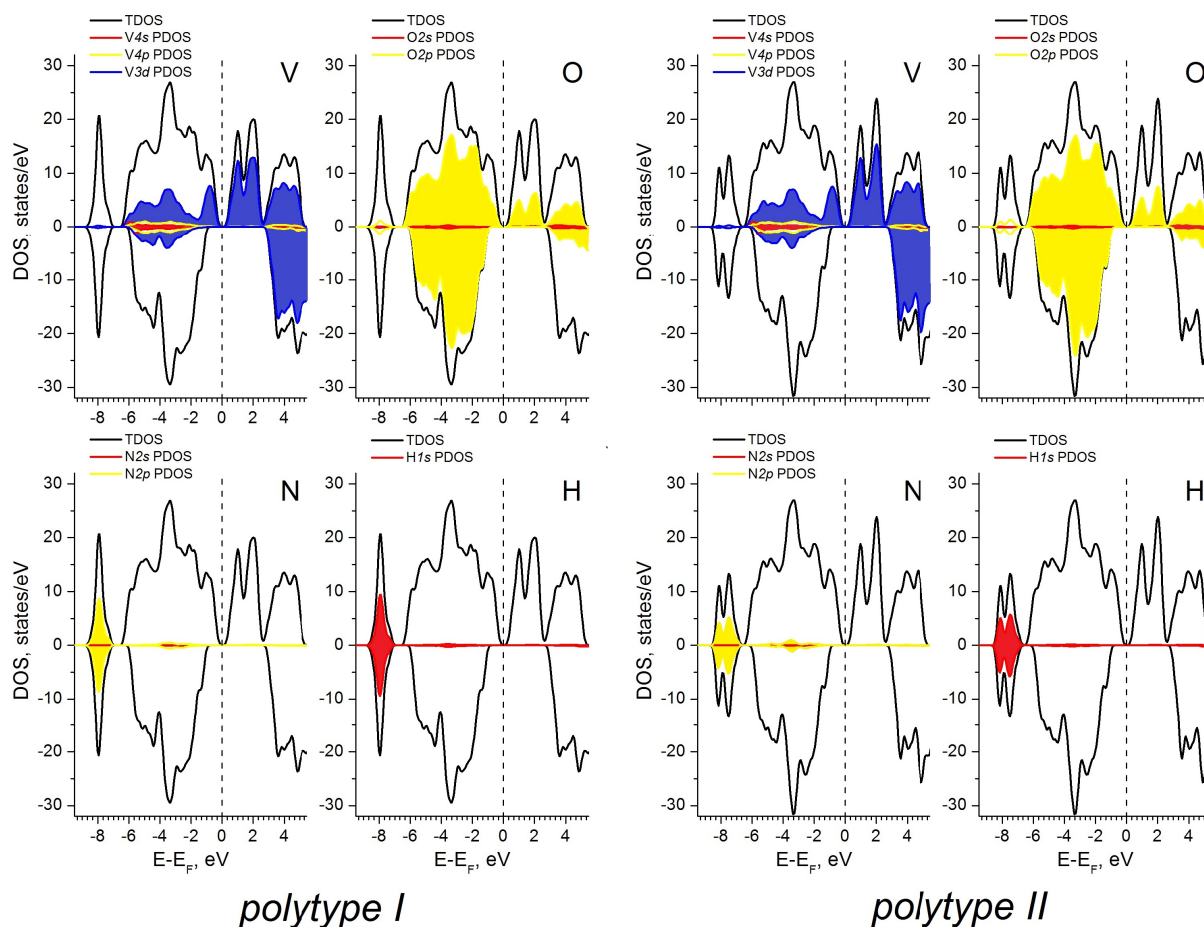


FIG. 5. Total and partial densities-of-states (DOS) for two polytypic  $\text{NH}_4\text{V}_3\text{O}_7$  phases. DFT calculations.

Analysis of the Mulliken charge distribution indicates that two groups of V atoms can be distinguished, with the charges  $+1.11$  and  $+1.14$  respectively. These groups differ in the environment of their second coordination shell. The first group of four V atoms is placed within the middle of a  $\text{V}_3\text{O}_7$  sextuple ribbon as  $\text{VO}_6$  octahedra with shared edges. The second group of two V atoms is placed at the edges of this ribbon as  $\text{VO}_6$  octahedra sharing their vertices with equivalent  $\text{VO}_6$  octahedra of the neighboring ribbon. The coordination polyhedra of the latter group have a heavily distorted geometry, with one of V–O distances at  $2.44$  Å, the largest of the group. The spin-polarization calculations indicate a magnetization of the compound with the spin density redistribution at the V atoms. The estimated magnetic moments within aforementioned groups of V atoms were found to be  $2.40$  and  $1.73 \mu_B$ .

The charge distribution among the O atoms is wider, yet, a few groups of atoms can be distinguished, depending mainly on the coordination number:  $-0.42$ ,  $-0.49 \dots -0.60$  and  $-0.54 \dots -0.66$  for O atoms within vanadyl groups, for bridging double and for triple coordinated O atoms, respectively. The charges on every N and every H atom are equal to  $-0.68$  and  $+0.28$ , respectively, which amounts to the total formal charge of  $\text{NH}_4^+$  cation as equal to  $+0.44$ .

The results of DFT calculations for polytype II show that the overall qualitative picture of the density of states is preserved (Fig. 5). Both considered  $\text{NH}_4\text{V}_3\text{O}_7$  polytypes should be magnetic semiconductors. In general, the charge distribution and the DOS picture of both polytypes explicitly correspond to the formation of covalent V–O and N–H bonding within anionic  $\text{V}_3\text{O}_7$  framework and ammonium  $\text{NH}_4$  cations. The relative position of dominating  $\text{V}3d\text{--O}2p$  and  $\text{N}2p\text{--H}1s$  overlaps in the valence band gives evidence for a highly versatile  $\text{V}_3\text{O}_7$  network for redox reactions as well as a low ability of  $\text{NH}_4$  cations for reduction, e.g. using alkali metal atoms.

#### 4. Summary

In summary, a facile chimie douce route was evaluated to produce highly textured product of pure ammonium trivanadate  $\text{NH}_4\text{V}_3\text{O}_7$  from the corresponding metavanadate  $\text{NH}_4\text{VO}_3$  as precursor and citric acid  $\text{C}_6\text{H}_8\text{O}_7$  as a mild reductant. The intricate structure of the product was characterized by the combination of experimental SEM, XRD and computational DFT techniques, which uncover a complex structural hierarchy of synthesized  $\text{NH}_4\text{V}_3\text{O}_7$ .

SEM data has revealed the microstructure as an aggregation of spherical-like particles with the diameters of  $\sim 30 \mu\text{m}$ , assembled of stochastically oriented nanoplatelets with thicknesses of  $50 - 200 \text{ nm}$  and edge lengths up to  $2 \mu\text{m}$ . Yet, the values of the lattice parameters derived using recent XRD data and upon assumption of crystalline  $\text{NH}_4\text{V}_3\text{O}_7$  were found to be quite different from previous experimental and recent DFT data. Assuming a domain-like organization of synthesized  $\text{NH}_4\text{V}_3\text{O}_7$ , X-ray diffractograms have been routinely simulated for a wide range of the size and for several possible domain morphologies. Indeed, it suggests even a more deep organization of  $\text{NH}_4\text{V}_3\text{O}_7$  microparticles at the nanoscopic level. Most likely, the lattice of  $\text{NH}_4\text{V}_3\text{O}_7$  studied in this work tends towards the formation of low-energy dislocations or twinning along  $[010]$  direction, which is a prerequisite for the emergence of needle-like nanodomains or a very rich polytypism.

A further study of  $\text{NH}_4\text{V}_3\text{O}_7$  by means of high-resolution electron microscopy could prove the structural hierarchy in more detail. Though, relying on DFT calculations, we predict that the electronic and chemical properties of layered  $\text{NH}_4\text{V}_3\text{O}_7$  would be not altered, even by possible domain-like organization. Two most prominent  $\text{NH}_4\text{V}_3\text{O}_7$  polytypes should be magnetic semiconductors with band gaps of  $\sim 0.8 \text{ eV}$ . Irrespective of their lattice arrangement, the anionic  $\text{V}_3\text{O}_7$  framework should be highly versatile in redox reactions, while  $\text{NH}_4^+$  cations should demonstrate a low ability for reduction, e.g. with alkali metal atoms.

#### Acknowledgments

The support from the Ministry of Science and Education of Russian Federation (unique project identifier RFMEF161314X0002) is gratefully acknowledged.

#### References

- [1] Wu C., Xie Y. Promising Vanadium Oxide and Hydroxide Nanostructures: From Energy Storage to Energy Saving. *Energy & Environmental Science*, 2010, **3**, P. 1191–1206.
- [2] Hellmann I., Zakharova G.S., et al. Static Susceptibility and Heat Capacity Studies on  $\text{V}_3\text{O}_7 \cdot \text{H}_2\text{O}_7$  Nanobelts. *Journal of Magnetism and Magnetic Materials*, 2010, **322**, P. 878–881.

- [3] Strelcov E., Lilach K., Kolmakv A. Gas Sensor Based on Metal-Insulator Transition in VO<sub>2</sub> Nanowire Thermistor. *Nano Letters*, 2009, **9**, P. 2322–2326.
- [4] Wang Y., Cao G.Z., Synthesis and Enhanced Intercalation Properties of Nanostructured Vanadium Oxides. *Chemistry of Materials*, 2006, **18**, P. 2787–2804.
- [5] Balakhonov S.V., Ivanov V.K., Baranchikov A.E., Churagulov B.R. A comparative analysis of physicochemical properties of vanadium-oxide nanomaterials fabricated via hydrothermal and microwave-hydrothermal methods. *Nanosystems: physics, chemistry, mathematics*, 2012, **3**, P. 66–74.
- [6] Rao K.J., Ramakrishnan P.A., Gadagkar R. Microwave Preparation of Oxide Bronzes. *Journal of Solid State Chemistry*, 1999, **148**, P. 100–107.
- [7] Xu Y., Han X.S., et al. Pillar Effect on Cyclability Enhancement for Aqueous Lithium Ion Batteries: a New Material of  $\beta$ -vanadium bronze M<sub>0.33</sub>V<sub>2</sub>O<sub>5</sub> (M = Ag, Na) nanowires. *Journal of Materials Chemistry*, 2011, **21**, P. 14466–14472.
- [8] Oka Y., Yao T., Yamamoto N. Crystal Structures and Lattice Distortions of  $\sigma$ -Type Layered Vanadium Bronzes:  $\sigma$ -M<sub>0.25</sub>V<sub>2</sub>O<sub>5</sub>·H<sub>2</sub>O (M=Mg, Co, Ni). *Journal of Solid State Chemistry*, 1999, **144**, P. 181–187.
- [9] Wu X., Tao Y., Dong L., Hong J. Synthesis and Characterization of Self-ling (NH<sub>4</sub>)<sub>0.5</sub>V<sub>2</sub>O<sub>5</sub> Nanowires. *Journal of Materials Chemistry*, 2004, **14**, P. 901–904.
- [10] Wang H., Huang K., et al. (NH<sub>4</sub>)<sub>0.5</sub>V<sub>2</sub>O<sub>5</sub> Nanobelt with Good Cycling Stability as Cathode Material for Li-ion Battery. *Journal of Power Sources*, 2011, **196**, P. 5645–5650.
- [11] Zhang K.-F., Zhang G.-Q., et al. Large Scale Hydrothermal Synthesis and Electrochemistry of Ammonium Vanadium Bronze Nanobelts. *Journal Power Sources*, 2006, **157**, P. 528–532.
- [12] Wang N., Chen W., Mai L., Dai Y. Selected-Control Hydrothermal Synthesis and Formation Mechanism of 1D Ammonium Vanadate. *Journal of Solid State Chemistry*, 2008, **181**, P. 652–657.
- [13] Zhou R., Zhang Z., et al. Oriented Free-Standing Ammonium Vanadium Oxide Nanobelt Membranes: Highly Selective Absorbent Materials. *Chemistry – A European Journal*, 2010, **16**, P. 14307–14312.
- [14] Ren T.-Z., Yuan Z.-Y., Zou X. Crystal Growth of Mixed-Valence Ammonium Vanadates. *Crystal Research and Technology*, 2007, **42**, P. 317–320.
- [15] Trombe J.C., Szajwaj O., Salles P., Galy J. Synthesis of New Mixed Valence Compounds MV<sup>5+</sup>V<sub>2</sub><sup>4+</sup>O<sub>7</sub> (M = NH<sub>4</sub>, K): Crystal Structure of NH<sub>4</sub>V<sub>3</sub>O<sub>7</sub> and Electrical Properties of KV<sub>3</sub>O<sub>7</sub>. *Journal of Solid State Chemistry*, 2007, **180**, P. 2102–2109.
- [16] Theobald F.R., Theobald J.-G., Vedrine J.C., Clad R., Renard J. Crystal Growth, Structure, Electron Paramagnetic Resonance and Magnetic Properties of (NH<sub>4</sub>)<sub>2</sub>V<sub>3</sub>O<sub>8</sub>. *Journal of Physics and Chemistry of Solids*, 1984, **45**, P. 581–587.
- [17] Liu G., Greedan J.E. Magnetic Properties of Fresnoite-Type Vanadium Oxides: A<sub>2</sub>V<sub>3</sub>O<sub>8</sub> (A = K, Rb, NH<sub>4</sub>). *Journal of Solid State Chemistry*, 1995, **114**, P. 499–505.
- [18] Fei H., Shen Z., et al. Flower-like (NH<sub>4</sub>)<sub>0.83</sub>Na<sub>0.43</sub>V<sub>4</sub>O<sub>10</sub>·0.26H<sub>2</sub>O Nano-structure for Stable Lithium Battery Electrodes. *Journal of Power Sources*, 2009, **189**, P. 1164–1166.
- [19] Fei H.-L., Shen Z.R., et al. Novel Bi-Cation Intercalated Vanadium Bronze Nano-structures for Stable and High Capacity Cathode Materials. *Electrochemistry Communications*, 2008, **10**, P. 1541–1544.
- [20] Hohenberg P., Kohn W. Inhomogeneous Electron Gas. *Physical Review B*, 1964, **136**, P. 864–871.
- [21] Ordejon P., Artacho E., Soler J.M. Self-Consistent Order-N Density-Functional Calculations for Very Large Systems. *Physical Review B*, 1996, **53**, R10441.
- [22] Soler J.M., Artacho E., et al. The SIESTA Method for ab initio Order-N Materials Simulation. *Journal of Physics: Condensed Matter*, 2002, **14**, P. 2745–2779.
- [23] Perdew J.P., Burke K., Ernzerhof M. Generalized Gradient Approximation Made Simple. *Physical Review Letters*, 1996, **77**, P. 3865–3868.
- [24] Troullier N., Martins J.L. Efficient Pseudopotentials for Plane-Wave Calculations. *Physical Review B*, 1991, **43**, P. 1993–2006.
- [25] Monkhorst H.J., Pack J.D. Special Points for Brillouin-Zone Integrations. *Physical Review B*, 1976, **13**, P. 5188–5192.
- [26] Moreno J., Soler J.M. Optimal Meshes for Integrals in Real- and Reciprocal-Space Unit Cells. *Physical Review B*, 1992, **45**, P. 13891–13898.
- [27] Caglioti G., Paoletti A.B., Ricci F.P. Choice of Collimators for a Crystal Spectrometer for Neutron Diffraction. *Nuclear Instruments and Methods in Physics Research*, 1958, **3**, P. 223.